



# Coherent beam combining of seven fiber chirped-pulse amplifiers using an interferometric phase measurement

ANKE HEILMANN,<sup>1,\*</sup> JÉRÉMY LE DORTZ,<sup>2</sup> LOUIS DANIAULT,<sup>1</sup> IHSAN FSAIFES,<sup>1</sup> SÉVERINE BELLANGER,<sup>1</sup> JÉRÔME BOURDERIONNET,<sup>2</sup> CHRISTIAN LARAT,<sup>2</sup> ERIC LALLIER,<sup>2</sup> MARIE ANTIER,<sup>3</sup> ERIC DURAND,<sup>3</sup> CHRISTOPHE SIMON-BOISSON,<sup>3</sup> ARNAUD BRIGNON,<sup>2</sup> AND JEAN-CHRISTOPHE CHANTELOUP<sup>1</sup>

<sup>1</sup>*Ecole Polytechnique, Université Paris-Saclay, 91128 Palaiseau Cedex, France*

<sup>2</sup>*Thales Research & Technology, 1 avenue Augustin Fresnel, 91767 Palaiseau Cedex, France*

<sup>3</sup>*Thales LAS France SAS, 2 avenue Gay Lussac, 78995 Elancourt Cedex, France*

\*[anke.heilmann@polytechnique.edu](mailto:anke.heilmann@polytechnique.edu)

**Abstract:** Coherent beam combining in tiled-aperture configuration is demonstrated on seven femtosecond fiber amplifiers using an interferometric phase measurement technique. The residual phase error between two fibers is as low as  $\lambda/55$  RMS and a combination efficiency of 48% has been achieved. The combined pulses are compressed to 216 fs, delivering 71 W average power at a repetition rate of 55 MHz. Operating the laser system in a nonlinear regime with an estimated  $B$ -integral of 5 rad yields a combining efficiency of 45% with the same phase stability. These results pave the way to very large high-power and high energy coherent beam combining systems.

© 2018 Optical Society of America under the terms of the [OSA Open Access Publishing Agreement](#)

## 1. Introduction

Ultrafast high power lasers are used in various fields ranging from fundamental science to industrial applications. Among the different amplifying architectures fiber lasers are of special interest due to their advantageous characteristics such as excellent beam quality, high efficiency, good thermal handling, and a certain robustness and ease of use. However, their peak powers are limited due to the occurrence of nonlinear effects which affect the temporal pulse quality and in the worst case damage the fiber itself. A promising method to overcome this limitation is coherent beam combining (CBC) [1], a technique which consists in the spatial splitting of the beam into  $N$  sub-beams prior to amplification, and the subsequent recombination of the amplified beams. For this recombination to be efficient, the phases of the sub-beams need to be adjusted such that they match one another [2, 3]. In this way, the peak and average powers can theoretically be increased by a factor of  $N$ , far beyond what is possible with a single fiber, while keeping the nonlinear effects at a constant level.

Applications in the field of high energy physics, such as particle acceleration, would benefit from the high average powers provided by fiber laser systems, but would require pulse energies of about 10 J [4]. Considering the millijoule level of a single emitter, this corresponds to combining up to 10,000 fibers. Hence, highly scalable CBC architectures need to be investigated. The XCAN (Coherent Amplification Network) project, a collaboration between the Ecole Polytechnique and Thales, aims at designing and demonstrating a highly scalable CBC architecture in the femtosecond regime including 61 fibers as a target point.

CBC can be performed either in filled-aperture or in tiled-aperture configuration. The former exhibits higher combining efficiencies [5, 6] but often involves multiple combining elements in cascade, so that the system complexity increases with the number of fibers. Recently, the two-by-two recombination of 16 beams has been demonstrated with only two segmented mirrors,

thus lightening the filled-aperture complexity for a consequent number of channels [7]. On the other hand, aperture tiling leads to lower combining efficiencies but allows the easy stacking of a great number of fibers and performing beam combination in one single step without any combining elements [8].

Besides, the phase matching technique needs to be carefully designed in order to address a large number of fibers. Various phase detection and control methods, such as frequency tagging [6, 9] or Hänsch-Couillaud interferometry [10], have demonstrated good efficiencies and robustness in the femtosecond regime for a moderate number of fibers. Recently, a specific implementation of LOCSET has shown a drastic increase of the number of channels that can be addressed with a limited frequency-tagging spanning [7]. However, CBC is still performed in a two-by-two configuration with at least two detectors at different points in the setup. Besides, it has been shown that an interferometric method is able to perform a collective phase measurement using only one frame of a single fast camera. Moreover, this method is theoretically able to handle the CBC of up to 10,000 fibers [11], and its implementation in the femtosecond regime has been demonstrated within the XCAN project using 19 passive fibers [12].

In this paper, we report on the CBC of seven femtosecond fiber chirped-pulse amplifiers operating at high average power, as a first step of the 61-fiber XCAN system. This is to our knowledge the first demonstration of a highly scalable CBC of femtosecond fiber amplifiers involving the tiled-aperture geometry along with the interferometric phase measurement and control.

## 2. Numerical simulations

The tiled-aperture architecture of the XCAN system consists in stacking  $N$  fibers in a hexagonal array, which guarantees highest aperture filling and therefore highest combining efficiencies. The output beams are collimated by a hexagonal microlens array (MLA) itself made of hexagonal microlenses. Their common image focal plane defines the near field position of the tiled-aperture. CBC is performed without any combining elements in the far field, which is given as the spatial Fourier transform of the near field. Thus, the combined beam corresponds to the main lobe of the far field pattern, and the combining efficiency  $\eta$  is defined as the average power in this main lobe divided by the overall average power delivered by the fiber amplifiers.

This architecture entails different types of combining efficiency losses. First, at the MLA plane, the width of an individual beam can be larger than the microlens diagonal, so that the edges of the beam are not collimated by the respective microlens. This microlens clipping leads thus to a power loss in the system, which reduces the combining efficiency. Moreover, the periodic intensity distribution of the composite beam in the near field gives rise to secondary lobes surrounding the central lobe in the far field, resulting in a further efficiency decrease. Finally, misalignments in the fiber array and disparities in the spectral content of the femtosecond pulses deteriorate the far-field profile, leading to additional efficiency losses.

In order to estimate the impact of the microlens clipping on the combination efficiency, we define the microlens fill factor  $\tau_r$  as the ratio between the diameter of the Gaussian beam at  $1/e^2$  of its intensity profile maximum and the MLA pitch which equals the short diagonal of the hexagonal microlenses. For increasing fill factors, the near field gets more homogeneous, resulting in a higher amount of power in the main lobe of the far field. However, the beams get also clipped by the MLA such that the effective microlens transmission  $t_{\mu\text{-lens}}$  decreases. The total combination efficiency  $\eta$  is thus a trade-off between aperture filling and microlens clipping, where the maximum efficiency of  $\eta = 67\%$  is obtained for a fill factor of  $\tau_r = 0.93$  [cf. Fig. 1]. These results are valid for any number of channels, even for the smallest hexagon at  $N = 7$  beams. In the following, the fill factor is set to this optimal value, representing the ideal case.

We then estimate the impact of spatial misalignments and spectral disparities among the beams on the combination efficiency. Indeed, such perturbations distort the far-field profile so that

the power contained in the ideal main lobe area decreases. Since the XCAN project aims at combining  $N = 61$  fibers, this number of beams is used in the simulations.

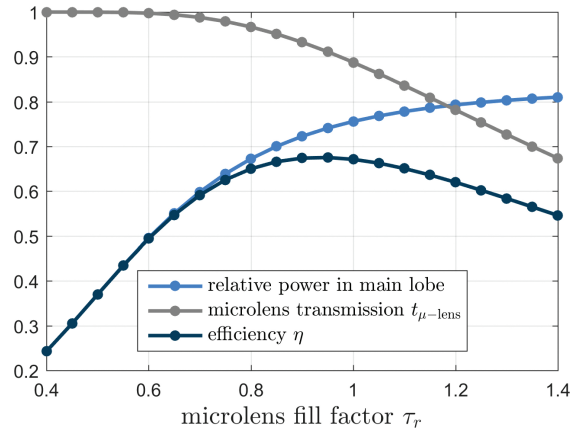


Fig. 1. Combination efficiency as a function of microlens transmission and relative power contained in the main lobe of the far field.

As stated above,  $\eta$  is highly sensitive to imprecisions on the alignment of the fiber array. We thus simulate the fiber positioning and beam pointing errors using the geometric parameters of our experimental fiber array. The mode field diameter of the fiber is set to  $30\ \mu\text{m}$  and the array pitch to  $3.2\ \text{mm}$ . The optimal fill factor yields a microlens focal length of  $65.7\ \text{mm}$  assuming a Gaussian beam shape with  $M^2 = 1.15$  for all the emitters. We first apply random errors drawn from a Gaussian distribution on the lateral positioning of the 61 fibers and estimate the corresponding combining efficiency. If we set the maximum tolerable drop in efficiency to one percentage point, that is, from 67% to 66%, the standard deviation of these errors must not exceed  $1\ \mu\text{m}$ . This tolerance represents about 0.03% of the array pitch and is one of the most critical alignment parameters in our setup. In the same way, errors on the tilts of the fibers should be kept below  $2\ \text{mrad}$  RMS, at about 5% of the microlens numerical aperture. Finally, the longitudinal distances between the fiber output and the MLA should not vary by more than  $0.08\ \text{mm}$  RMS, which roughly corresponds to 10% of the Gaussian beam Rayleigh range of the fiber output. These results are in good agreement with previously published simulations on the CBC of CW lasers [13]. Besides, reducing the number of fibers to  $N = 7$  yields very similar results for the spatial errors.

Furthermore, we study the characteristics specific to the femtosecond regime and their impact on the combining efficiency. Including the spectral dimension in our model, the electric field of one beam reads:

$$E(x, y, \omega) = E_{\text{spatial}}(x, y) \times E_0(\omega)e^{i\varphi(\omega)} \quad (1)$$

where  $E_{\text{spatial}}(x, y)$  is the spatial profile of the beam,  $E_0(\omega)$  the spectral amplitude of the pulse and  $\varphi(\omega)$  its spectral phase. Both terms  $E_{\text{spatial}}(x, y)$  and  $E_0(\omega)$  are normalized quantities. We assume a Gaussian spectrum  $E_0(\omega) = \exp(-(\omega - \omega_0)^2 / (2\Delta\omega_0^2))$  centered at  $\omega_0$  with a standard deviation of  $\Delta\omega_0$ . We choose parameters close to our laser system and set the central wavelength to  $\lambda_0 = 1032\ \text{nm}$  and the intensity FWHM to  $7\ \text{nm}$ , which corresponds to a pulse duration of  $\Delta t = 223\ \text{fs}$ . In the following, the spectral amplitude  $E_0(\omega)$  remains equal for all the beams and their spatial arrangement is supposed to be ideal so that we only take the spectral phase effects into account.

First, we study the effect of dispersion discrepancies between the beams on the combining

efficiency. The corresponding spectral phase can be expressed as:

$$\varphi(\omega) = \varphi_0 + \varphi_1(\omega - \omega_0) + \frac{\varphi_2}{2}(\omega - \omega_0)^2 + \mathcal{O}\left((\omega - \omega_0)^3\right) \quad (2)$$

where  $\varphi_0$  is a phase offset,  $\varphi_1$  a delay and  $\varphi_2$  the chirp of the pulses. Since the combining efficiency is only sensitive to spectral discrepancies among the beams, the average value of each spectral phase coefficient is set to zero.

The phase offset  $\varphi_0$  is independent of  $\omega$ , so that its impact on the combining efficiency can be calculated using the same numerical model as for the spatial errors. However, for the higher order spectral phase components, a separate far field needs to be modeled for every frequency increment, and the corresponding spectral efficiency  $\eta(\omega)$  is calculated. The overall combining efficiency is then given as the sum of  $\eta(\omega)$  weighted by the spectral intensity  $|E_0(\omega)|^2$ , and the total far field is reconstructed by summing the intensities of the frequency-dependent far fields.

Considering the expression of the spectral phase, the central frequency component always yields an ideal far field. However, for frequencies at the edge of the spectrum the far field pattern gets more arbitrary, with less power concentrated in the main lobe and a more pronounced speckle pattern around it. This behavior is illustrated in Fig. 2 for three different wavelengths ranging from the center to the edge of the spectrum for a first order spectral phase distribution. As a consequence, for large spectral phase mismatches, the power contained in the central lobe gets significantly reduced for the edge frequencies, leading to an effective spectral narrowing of the combined beam. This results in increasing the minimum duration of the combined pulse, so that its highest achievable peak power is reduced. As CBC in the femtosecond regime is intended for peak-power scaling, it is useful to consider the peak-power efficiency, defined as the ratio between the peak power of the Fourier transform-limited (FTL) combined pulse and  $N$  times the common peak power of the FTL pulses to combine. This quantity takes into account the average power efficiency as well as the spectral narrowing of the combined pulse.

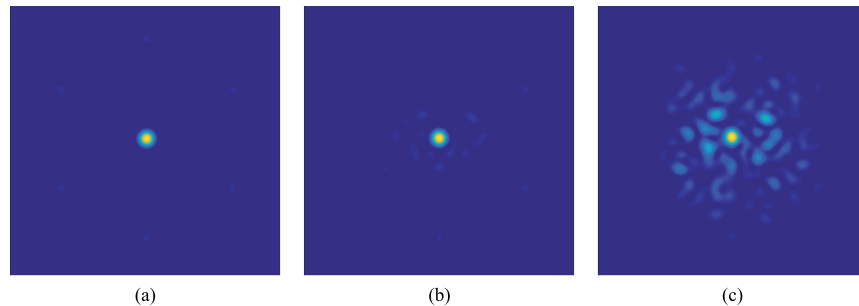


Fig. 2. Example far fields for three different wavelengths from the center (a) to the edge (c) of the spectrum. On each beam, a spectral phase of first order randomly drawn from a Gaussian distribution with standard deviation  $\Delta\varphi_1 = 250$  fs is applied.

The curves shown in Fig. 3 depict the efficiency losses in terms of average and peak power for  $N = 61$  beams if an arbitrary phase drawn from a Gaussian distribution with standard deviation  $\Delta\varphi_{0,1,2}$  is introduced on each individual beam. Since this is a statistical process, 50 runs were executed for each error, and the given efficiencies are the mean of the 50 individual results, whereas the error bars represent their standard deviation.

In order to limit the efficiency losses in average power to one percentage point as fixed above,  $\Delta\varphi_0$  must not vary by more than  $\pi/25$  rad or  $\lambda/50$  RMS. Since the phase offsets fluctuate continuously in a laboratory environment due to thermal and acoustic noises, it is necessary to implement a feedback algorithm which can ensure a very high quality phase locking. In contrast, the pulse arrival time  $\varphi_1$  and the chirp  $\varphi_2$  do not need to be corrected actively since they mainly

depend on the total length of fiber in each channel. Hence, a matching of optical path length is necessary, and in order to meet the one percentage point requirement stated above, it needs to be accurate enough to limit the relative delays between the pulses to 22 fs RMS. This corresponds to an optical path difference of 6  $\mu\text{m}$  or 10% of the coherence length of the pulses. In the same way, second order phase mismatches should be limited to  $5 \times 10^3 \text{ fs}^2$  RMS, corresponding to a fiber length mismatch of 25 cm. It is noteworthy that for an efficiency drop of one percentage point, the dimensionless coefficients  $\Delta\varphi_1/\Delta t$  and  $\Delta\varphi_2/\Delta t^2$  have the same order of magnitude of about 0.1, and remain independent of the spectral width of the pulse. However, the combining efficiency drops less drastically for higher orders of the spectral phase as shown in Fig. 3.

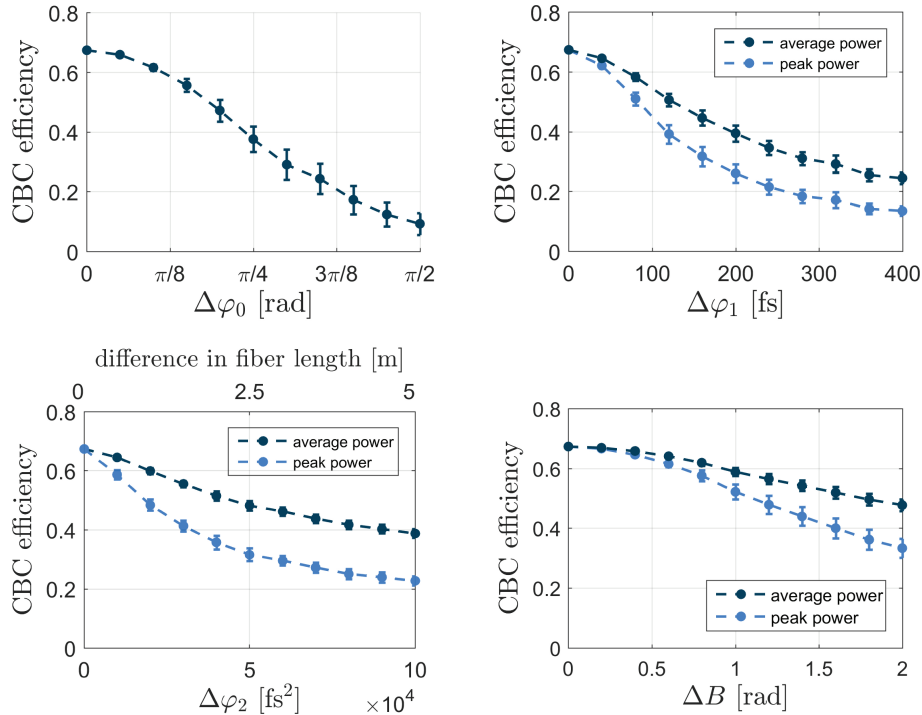


Fig. 3. Coherent combination efficiency for average and peak power of 61 beams as a function of errors on the spectral phase of each individual beam. Their spatial arrangement is supposed to be ideal.

Furthermore, we study the impact of nonlinear effects experienced by the pulses on the combining efficiency. In our context, we consider chirped-pulse amplification at high energy such that self-phase modulation (SPM) can arise. As we assume highly stretched pulses, the effect of SPM can be approximated in the spectral domain by a phase term  $\varphi_{\text{NL}}(\omega) = B|E_0(\omega)|^2$  where  $B$  is the  $B$ -integral experienced by the pulse. The effect of SPM on the combining efficiency can thus be treated the same way as for the linear regime by adding a nonlinear phase term  $\varphi_{\text{NL}}(\omega) = (B + \Delta B)|E_0(\omega)|^2$  on each channel, where  $B$  represents the average  $B$ -integral of all the channels and  $\Delta B$  is a random fluctuation arising from different amplification conditions such as seed or pump power discrepancies. We assume that the spectral amplitude is constant among the beams and that  $B > |\Delta B|$  so that negative total  $B$ -integrals are avoided. However, the average value  $B$  has no impact on the combining efficiency since it is common to all the beams. Moreover, considering that in typical femtosecond CBC experiments, the zeroth and first orders of the spectral phase can be compensated by a phase locking technique and a fine delay adjustment, we remove the corresponding components from the nonlinear phase before applying it to the beams.

The remaining differences in nonlinear phase should not exceed  $\Delta B = 0.32$  rad in order to limit the decrease in combining efficiency to one percentage point.

It should be noted that errors in the spectral domain have a fundamentally different effect than the spatial ones. For the latter, it is possible to achieve complete destructive interference in the area of the main lobe of an ideal far field, so that the calculated combining efficiency can drop to zero. In contrast, spectral errors degrade the coherence of the far field, with the extreme case of an incoherent superposition of the individual beams. Hence, there is always a certain amount of power confined in the area of the ideal main lobe and the combining efficiency cannot fall below a certain minimum value. Therefore, the combining efficiency converges to a non-zero asymptotic value for increasing spectral disparities. However, this asymptotic value is highly dependent on the number  $N$  of beams to combine. Indeed, by increasing  $N$ , the near field area gets larger such that the ideal main lobe area in the far field gets smaller, whereas the size of the incoherent superposition of the beams is unchanged. Hence, the fraction of power of the incoherent beam encircled in the ideal main lobe area strongly decreases as well. As an example, for  $N = 7$  and  $N = 61$ , the ideal combining efficiency is nearly the same at about 67% as stated above, but the asymptotic value of the combining efficiency obtained for very large spectral discrepancies falls down to 38% and 4%, respectively. Therefore, the combining efficiency is more sensitive to spectral phase mismatches for higher numbers of beams to combine. Hence, in the case of seven fibers, the error tolerances are less demanding: a phase stabilization of  $\lambda/40$  RMS is sufficient, whereas relative errors of 0.15 can be tolerated on the first and second orders of the spectral phase. Furthermore, discrepancies in the  $B$ -integral can be as high as 0.46 rad.

The simulations presented in this section provide guidelines to design a tiled-aperture CBC experiment in the femtosecond regime with little effect of spatial and temporal errors on combining efficiency losses.

### 3. Experimental setup

A simplified schematic of our experimental setup is shown in Fig. 4. The master oscillator, a Mikan from Amplitude Systèmes, delivers 225 fs laser pulses at a repetition rate of 55 MHz. In a first step, the beam is coupled into a 3 m polarization-maintaining single mode fiber. This allows to use the spectral broadening of the self-phase modulation in order to partially compensate for the gain narrowing induced by subsequent amplification stages. Next, the spectrum is cut sharp between 1026 nm and 1041 nm by a chirped fiber Bragg grating (CFBG), which stretches the pulses to a duration of 500 ps. It is followed by a pulse shaper used to pre-compensate the dispersion accumulated all over the setup and common to all channels.

The beam is then split into eight sub-beams, each of which is passed through a phase and delay adjustment module ( $\Delta\varphi$ -boxes in Fig. 4). These elements were designed and manufactured for us by IDIL Fibres Optiques and consist of two stages: first, the phase is corrected in real time by a piezo-mechanical fiber stretcher adjusting the optical path length in a range of  $\pm 19$   $\mu\text{m}$ , which corresponds to phase shifts of  $\pm 18.4\lambda$ . Second, a motorized free space variable optical delay line allows the fine adjustment of the pulse arrival time within a range of  $\pm 3$  cm or  $\pm 90$  ps, with 0.1  $\mu\text{m}$  or 0.3 fs increments. The fiber lengths of the eight channels are matched within a few cm such that residual delays between the pulses can fit into the delay lines range.

Two pulse-picking stages based on acousto-optic modulators (AOM) can be used to reduce the pulse repetition rate, thus increasing the output pulse energy in order to study CBC in nonlinear regime. The first stage in the common arm has a short response time of 6 ns and provides good extinction ratio and diffraction efficiency. The second one has a longer response time and is placed close to the end of the setup in order to manage the nonlinearity level of the whole system. These AOM have been provided by AA Optoelectronics along with an all-integrated control system including electronic pulse generators and RF drivers specifically designed for the XCAN architecture.

In order to compensate for power losses all over the laser chain, several 25 dB gain pre-amplifier stages delivering 100 mW of saturated output power, tailored for this laser system by Keopsys, a Lumibird Group company, are inserted all throughout the setup. The endmost ones use large mode area fibers to reduce nonlinear effects which occur in experiments conducted at lower pulse repetition rates.

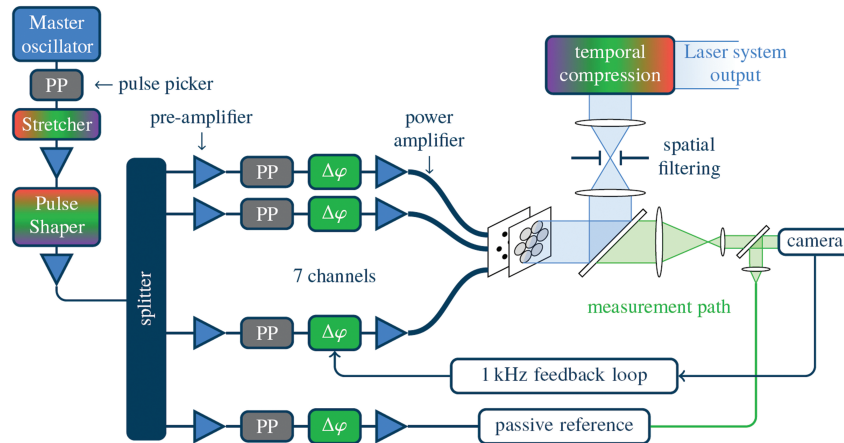


Fig. 4. Schematic of the experimental setup.

Except for the free space delay lines, our laser system operates with an all-polarization maintaining fiber front-end, thus guaranteeing a maximum of robustness and convenience of use.

Seven of the sub-beams are power amplified to a pump-limited average power of 25 W per channel using ytterbium-doped photonic crystal fibers (PCF) of 30  $\mu\text{m}$  mode field diameter, supplied by NKT Photonics and functionalized by Optical Engines. This functionalization includes three steps: first, a  $(2 + 1) \times 1$  pump + signal combiner followed by a mode field adapter is spliced at the fiber input, coupling the signal and pump beams efficiently into the PCF. Second, an end-cap is spliced to the end of the fiber in order to avoid surface damage. Third, a ferrule is placed at the fiber ending such that the fiber output mode is centered with respect to the outer diameter of the ferrule with a precision of a few microns.

In order to arrange the fibers accurately in a hexagonal array, the ferrules are inserted into a specifically designed high precision mechanical holder with a pitch of 3.2 mm. An estimation of the errors present on our setup yields standard deviations of 2.6  $\mu\text{m}$  on the fiber pitch, 0.7 mrad on the tilt and 0.2 mm on the focal distances. Moreover, the microlens fill factor was measured to be  $\tau_r = 0.7$  rather than the ideal value of 0.93, leading to an excess of power in the side lobes of the far field pattern. Indeed, the fill factor is highly sensitive to the mode field diameter and  $M^2$  of the beams and future experiments will involve an MLA more adapted to the actual fiber mode. Considering all these parameters, the maximal possible combination efficiency drops to  $\eta = 56\%$ , yielding a simulated far field as shown in Fig. 5(b).

CBC is performed using the interferometric phase measurement method described in [11]. The remaining eighth sub-beam is used as a plane wave reference for the real-time phase measurement. A small power fraction of the near field is imaged on a 1 kfps fast camera, where it is superposed with the plane wave. This allows the acquisition of seven interferograms on a single camera image, and the subsequent deduction of the relative phases between each channel and the reference beam. A 1 kHz feedback algorithm acting on the fiber stretchers is then implemented to stabilize these phases.

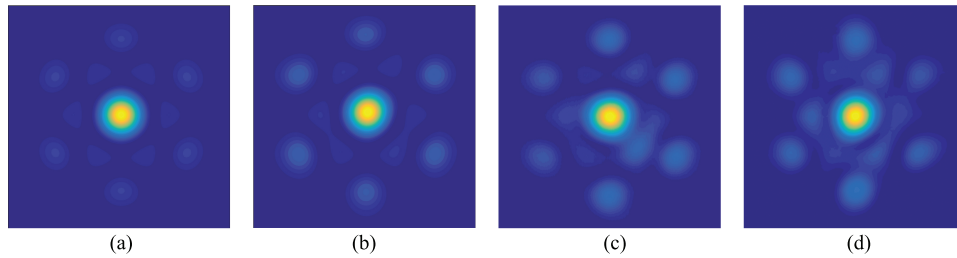


Fig. 5. (a) Simulation of an ideal far field (b), simulated far field including the measured microlens fill factor  $\tau_r$  and alignment errors in the fiber array, (c) measured far field in linear regime, (d) measured far field in nonlinear regime at an estimated  $B$ -integral of 5 rad. Each far field is normalized with respect to its maximum intensity.

#### 4. Experimental results

As stated in the previous section, the fiber lengths of all the channels are matched to a few cm. This ensures that there are no efficiency losses due to group velocity dispersion or higher order discrepancies considering the results of our simulations. When the overall system is thermalized, the delays are matched to less than 10 fs using the delay lines, by accurately maximizing the contrast of the interference fringes measured with the camera. Moreover, when the phase locking is enabled, the fiber stretchers also track the zero-delay position previously set by the delay lines. In this way, the impact of the overall group delay discrepancies on the combining efficiency can be neglected as well.

Then, we evaluate the quality of the phase locking by measuring the phase noise between two fiber amplifiers operating at full power in linear regime at a repetition rate of 55 MHz. The relative phase is retrieved by generating interference fringes between the two beams and simultaneously recording the interference states in quadrature using two independent photodiodes. Figure 6(a) shows the phase noise density of the measured relative phase in open and closed loops, respectively. The kHz feedback algorithm reduces the low-frequency noise by up to five orders of magnitude, yielding a residual phase error of  $\lambda/55$  RMS between two fibers. This is much better than the  $\lambda/40$  RMS tolerance on an individual emitter stated previously, so that the efficiency losses due to uncompensated phase offsets are negligible. We observe quite similar relative phase stabilities on other fiber pairs.

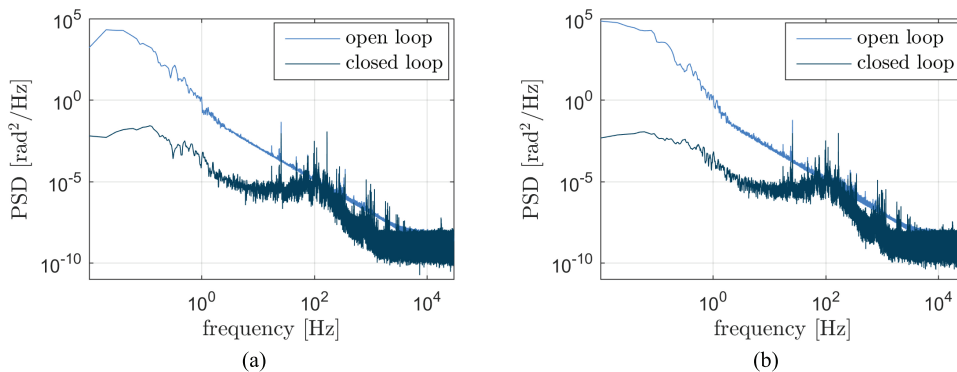


Fig. 6. Phase noise spectral density for open and closed loops in (a) linear and (b) nonlinear regime.

The system is then operated in closed loop in order to characterize the combined beam. We

obtain a far field as shown in Fig. 5(c). The good agreement between this measurement and the simulated far field shown in Fig. 5(b) confirms that spectral phase discrepancies have only a minor effect on the combination efficiency. We spatially filter the far field by truncating it at the first extinction of the ideal main lobe, and measure an output average power of 84 W, which is 49% of the total power of the far field. Taking into account the microlens transmission of  $t_{\mu\text{-lens}} = 98\%$  for our measured fill factor  $\tau_r = 0.7$ , the combination efficiency is given by  $\eta = 48\%$ . This corresponds to 86% of the simulated value stated above. The remaining difference might be due to a slightly overestimated microlens fill factor or an underestimation of the alignment errors in the fiber array.

We measure the power stability of the spatially filtered combined beam by focusing it on a photodiode. We obtain a power noise spectrum as shown in Fig. 7, with residual power variations as low as 1.7% RMS. Regarding the phase locking quality measured above, the power stability should be lower than 1% RMS according to our simulations. However, it is also highly sensitive to beam pointing instabilities considering the very small size of the filtering hole. Thus, special care has to be taken on the optomechanical elements redirecting the laser beam before the filtering process in order to improve the combined beam power stability.

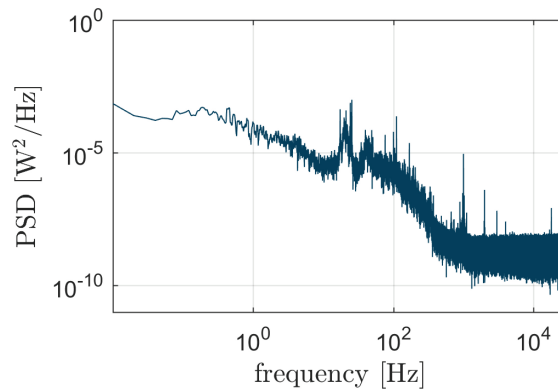


Fig. 7. Power noise spectrum of the combined beam.

Due to the hard cut intensity distribution in the near field, the amplitude of the combined beam in the far field is described by an Airy pattern clipped at the first zero [Fig. 8(a) and 8(b)]. However, the near field of the combined beam, obtained by an optical Fourier transform of the filtered beam, recovers a Gaussian-like shape [Fig. 8(c) and 8(d)]. The  $M^2$  beam quality is measured using the second-moment method, yielding an  $M^2$  of 1.10 on both the  $x$ -axis and  $y$ -axis. Figure 9 shows the second-moment values of the intensity profiles for different propagation distances around the near field image of the filtered far field. It is worth noting that the filtered beam has a quite similar behavior as a fundamental Gaussian beam, which is confirmed by the low  $M^2$  values.

Finally, the spatially filtered beam is temporally compressed using a 1760 l/mm multilayer-dielectric reflection grating pair. Based on the measured spectrum shown in Fig. 10(b), we calculate a Fourier transform-limited pulse duration of 212 fs and an autocorrelation function as shown in Fig. 10(a) with a FWHM of 293 fs. The measured autocorrelation trace exhibits a duration of 299 fs FWHM, showing that the compressed pulses are nearly Fourier transform-limited at about 216 fs pulse duration. We measure an average power of the combined beam of 71 W, which means that 82% of the power incident on the compressor is transmitted.

In order to evaluate the impact of nonlinear effects on the performances of our laser system, we reduce the pulse repetition rate to 2 MHz, operating thus in a nonlinear regime with an estimated  $B$ -integral of 5 rad. We first repeat the phase noise measurement and obtain the power

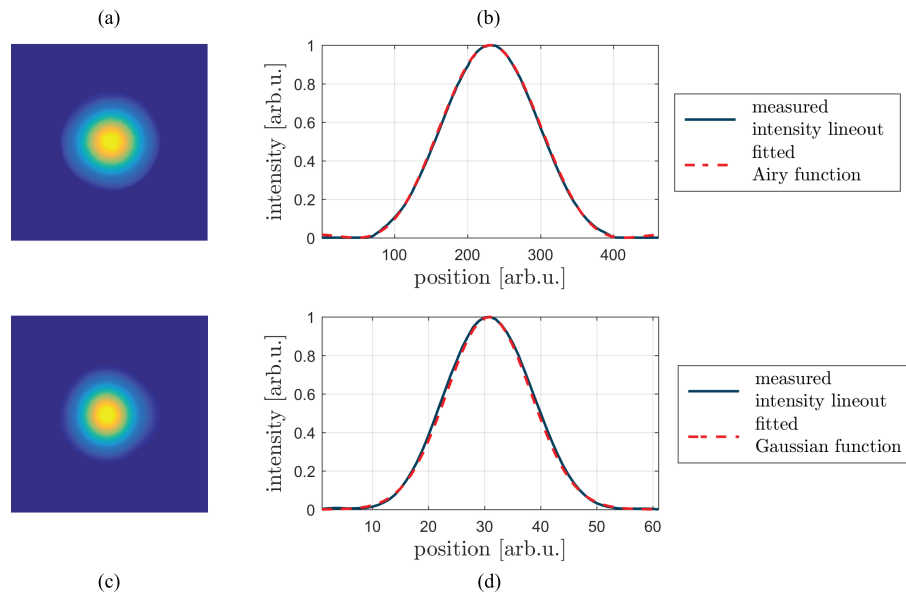


Fig. 8. (a) Combined beam in the far field, (b) lineout of the intensity profile and fitted Airy function, (c) near field of the combined beam obtained by optical Fourier transform of the spatially filtered far field, (d) lineout and fitted Gaussian function.

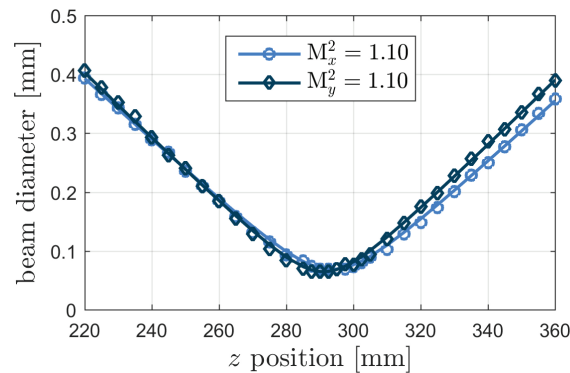


Fig. 9.  $M^2$  measurement of the combined beam.

spectral density shown in Fig. 6(b). The residual phase error of  $\lambda/55$  RMS is the same as the one observed in linear regime, showing that such nonlinear effects have no impact on the quality of the phase locking. Furthermore, the very similar phase noise spectral contents measured in open loop for both linear and nonlinear regimes confirm that the phase locking operates under the same conditions in both cases. Hence, the power stability of the beam remains similar in both cases as well.

The experimental far field obtained in closed loop in nonlinear regime is shown in Fig. 5(d). The slight halo around the central lobe is due to small mismatches in the nonlinear phases among the beams, which reduce the power contained in the main lobe to 82 W. The corresponding combining efficiency of  $\eta_{NL} = 45\%$  is thus slightly reduced with respect to the  $\eta = 48\%$  obtained in linear regime. Although it is difficult to accurately measure the  $B$ -integral experienced by each individual channel, it is possible to estimate the nonlinear discrepancies between them

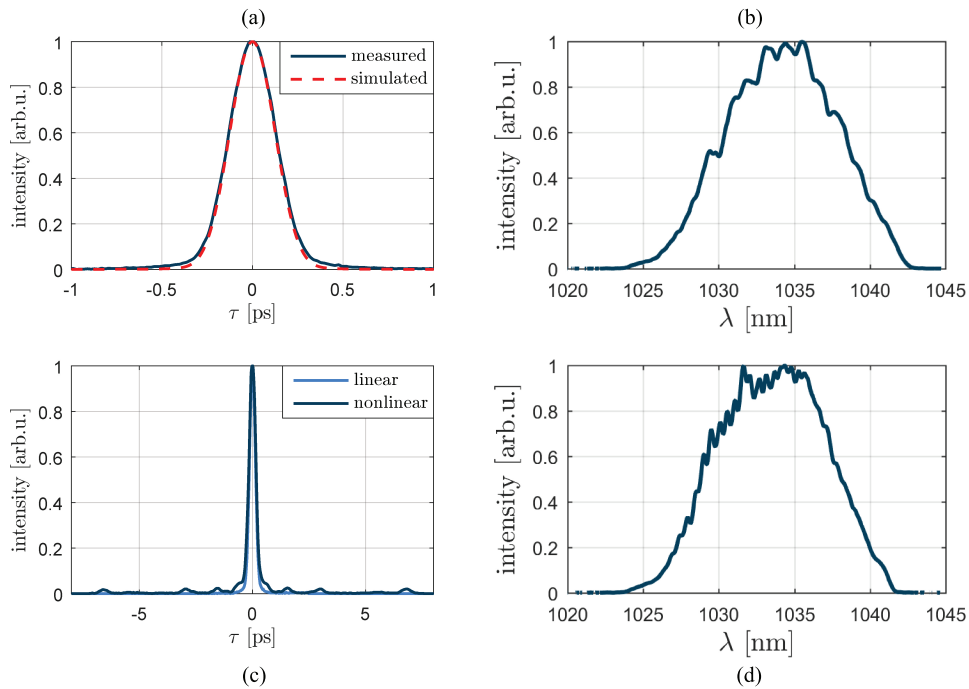


Fig. 10. Autocorrelation functions (left) and spectra (right) of the combined beam in linear (top) and nonlinear (bottom) regime.

using our simulations. Given the measured efficiency drop due to SPM, we derive an overall  $B$ -integral mismatch between the channels of about  $\Delta B = 0.8$  rad RMS, which is consistent with our amplification conditions and the high nonlinearity level of the system. Although the nonlinear effects lead to a slightly enhanced speckle pattern around the main lobe, they have no impact on the spatial qualities of the combined beam. This is due to the sharp spatial filtering of the far field which guarantees that the combined beam remains in its Airy shape and only its output power is reduced.

Temporal compression of the combined beam yields the autocorrelation trace shown in Fig. 10(c). For comparison, the autocorrelation trace measured in linear regime is shown as well. The onset of nonlinear effects leads to the emergence of secondary pulses and to a broadening of the main pulse autocorrelation trace to 350 fs FWHM. Since the combined spectrum FWHM is comparable to the one measured in linear regime, CBC itself cannot be responsible for the temporal pulse broadening. However, considering the all-fibered front-end, the dynamics of the pulse shaper is mostly used to compensate the strong excess of third-order dispersion due to the high stretcher/compressor mismatch. Thus, its remaining shaping capability is not sufficient enough to fully restore the FTL pulse duration in nonlinear regime. This issue can be easily solved by pre-compensating the fiber dispersion of the setup within the CFBG such that the dynamics of the pulse shaper can be fully available for compensating the nonlinear pulse distortions.

Nevertheless, these results show that nonlinear effects have only a minor impact on the combining efficiency and the quality of the phase locking. The limiting factor is thus the spectral distortion of the combined beam as it is the case in conventional laser systems.

## 5. Conclusion and outlook

In summary, we demonstrated the first coherent combination of seven fiber amplifiers using an interferometric phase measurement method. Operating in linear regime, a combination efficiency of 48% has been achieved, with a residual phase error between two fibers as low as  $\lambda/55$  RMS. The laser system delivers 71 W average power at a repetition rate of 55 MHz and with a pulse duration of 216 fs. In nonlinear regime, the same residual phase error and a slightly reduced combining efficiency of 45% were obtained. These very promising results show that our laser system is well adapted for the coherent combination of high power active fibers in tiled aperture configuration. Therefore, and since an upscaled version of our system will rely on the same scientific and technical principles, the implementation of 54 additional fibers and the operation of this final 61 fiber system will be demonstrated as a next step.

## Funding

French Ministry of Defense (Direction Générale de l'Armement); European Union's Horizon 2020 research and innovation program (654148 Laserlab-Europe).

## References

1. T. Y. Fan, "Laser beam combining for high-power, high-radiance sources," *IEEE J. Sel. Top. Quantum Electron.* **11**, 567–577 (2005).
2. S. J. Augst, T. Y. Fan, and A. Sanchez, "Coherent beam combining and phase noise measurements of ytterbium fiber amplifiers," *Opt. Lett.* **29**, 474–476 (2004).
3. G. D. Goodno, C.-C. Shih, and J. E. Rothenberg, "Perturbative analysis of coherent combining efficiency with mismatched lasers," *Opt. Express* **18**, 25403–25414 (2010).
4. G. Mourou, B. Brocklesby, T. Tajima, and J. Limpert, "The future is fibre accelerators," *Nat. Photonics* **7**, 258 (2013).
5. M. Müller, M. Kienel, A. Klenke, T. Gottschall, E. Shestae, M. Plötner, J. Limpert, and A. Tünnermann, "1 kw 1 mj eight-channel ultrafast fiber laser," *Opt. Lett.* **41**, 3439–3442 (2016).
6. M. Kienel, M. Müller, A. Klenke, J. Limpert, and A. Tünnermann, "12 mj kw class ultrafast fiber laser system using multidimensional coherent pulse addition," *Opt. Lett.* **41**, 3343–3346 (2016).
7. A. Klenke, M. Müller, H. Stark, F. Stutzki, C. Hupel, T. Schreiber, A. Tünnermann, and J. Limpert, "Coherently combined 16-channel multicore fiber laser system," *Opt. Lett.* **43**, 1519–1522 (2018).
8. J. Bourderionnet, C. Bellanger, J. Primot, and A. Brignon, "Collective coherent phase combining of 64 fibers," *Opt. Express* **19**, 17053–17058 (2011).
9. L. Daniault, M. Hanna, L. Lombard, Y. Zaouter, E. Mottay, D. Goular, P. Bourdon, F. Druon, and P. Georges, "Coherent beam combining of two femtosecond fiber chirped-pulse amplifiers," *Opt. Lett.* **36**, 621–623 (2011).
10. E. Seise, A. Klenke, S. Breitkopf, M. Plötner, J. Limpert, and A. Tünnermann, "Coherently combined fiber laser system delivering 120  $\mu$ j femtosecond pulses," *Opt. Lett.* **36**, 439–441 (2011).
11. M. Antier, J. Bourderionnet, C. Larat, E. Lallier, E. Lenormand, J. Primot, and A. Brignon, "kHz closed loop interferometric technique for coherent fiber beam combining," *IEEE J. Sel. Top. Quantum Electron.* **20**, 182–187 (2014).
12. J. Le Dortz, A. Heilmann, M. Antier, J. Bourderionnet, C. Larat, I. Fsaifes, L. Daniault, S. Bellanger, C. Simon Boisson, J.-C. Chanteloup, E. Lallier, and A. Brignon, "Highly scalable femtosecond coherent beam combining demonstrated with 19 fibers," *Opt. Lett.* **42**, 1887–1890 (2017).
13. C. Bellanger, A. Brignon, B. Toulon, J. Primot, F. Bouamrane, T. Bouvet, S. Megtert, L. Quetel, and T. Allain, "Design of a fiber-collimated array for beam combining," *Opt. Eng.* **50**, 025005 (2011).